


RESEARCH

Open Access



Controlled release of hydrogel-encapsulated mesenchymal stem cells-conditioned medium promotes functional liver regeneration after hepatectomy in metabolic dysfunction-associated steatotic liver disease

Naoya Kasahara^{1†}, Takumi Teratani^{2*†} , Junshi Doi³, Shinichiro Yokota¹, Kentaro Shimodaira¹, Yuki Kaneko¹, Hideyuki Ohzawa¹, Yasunaru Sakuma¹, Hideki Sasanuma¹, Yasuhiro Fujimoto⁴, Taizen Urahashi⁵, Hideyuki Yoshitomi⁵, Hironori Yamaguchi¹, Joji Kitayama¹ and Naohiro Sata¹

Abstract

Background Globally, prevalence of metabolic dysfunction-associated steatotic liver disease (MASLD) is increasing, and there is an urgent need to develop innovative therapies that promote liver regeneration following hepatectomy for this disease. Surgical excision is a key therapeutic approach with curative potential for liver tumors. However, hepatic steatosis can lead to delayed liver regeneration and higher post-operative complication risk. Mesenchymal stem cells-conditioned medium (MSC-CM) is considered a rich source of paracrine factors that can repair tissues and restore function of damaged organs. Meanwhile, hydrogels have been widely recognized to load MSC secretome and achieve sustained release. This study aimed to evaluate the therapeutic effect of hydrogel-encapsulated MSC-CM on liver regeneration following partial hepatectomy (PHx) in a rodent model of diet-induced hepatic steatosis.

Methods Male Lewis rats were fed with a methionine and choline-deficient diet. After 3 weeks of feeding, PHx was performed and rats were randomly allocated into two groups that received hydrogel-encapsulated MSC-CM or vehicle via the intra-mesenteric space of the superior mesenteric vein (SMV).

Results The regeneration of the remnant liver at 30 and 168 h after PHx was significantly accelerated, and the expressions of proliferating cell nuclear antigen were significantly enhanced in the MSC-CM group. MSC-CM treatment significantly increased hepatic ATP and β -hydroxybutyrate content at 168 h after PHx, indicating that MSC-CM fosters regeneration not only in volume but also in functionality. The number of each TUNEL- and cleaved caspase-3 positive nuclei in hepatocytes at 9 h after PHx were significantly decreased in the MSC-CM group, suggesting that MSC-CM suppressed apoptosis. MSC-CM increased serum immunoregulatory cytokine interleukin-10 and interleukin-13 at 30 h after PHx. Additionally, mitotic figures and cyclin D1 expression decreased and hepatocyte size increased in the MSC-CM group, implying that this mode of regeneration was mainly through cell hypertrophy rather than cell division.

[†]Naoya Kasahara and Takumi Teratani have contributed equally to this work.

*Correspondence:

Takumi Teratani
teratani@jichi.ac.jp

Full list of author information is available at the end of the article



This is a U.S. Government work and not under copyright protection in the US; foreign copyright protection may apply 2024. **Open Access** This article is licensed under a Creative Commons Attribution 4.0 International License, which permits use, sharing, adaptation, distribution and reproduction in any medium or format, as long as you give appropriate credit to the original author(s) and the source, provide a link to the Creative Commons licence, and indicate if changes were made. The images or other third party material in this article are included in the article's Creative Commons licence, unless indicated otherwise in a credit line to the material. If material is not included in the article's Creative Commons licence and your intended use is not permitted by statutory regulation or exceeds the permitted use, you will need to obtain permission directly from the copyright holder. To view a copy of this licence, visit <http://creativecommons.org/licenses/by/4.0/>.

Conclusions MSC-CM represents a novel therapeutic approach for patients with MASLD requiring PHx.

Keywords Non-alcoholic fatty liver disease, Hepatectomy, Liver regeneration, Adipose tissue-derived mesenchymal stem cells, Conditioned medium, Hydrogel, Controlled release, Regenerative medicine

Background

Globally, metabolic dysfunction-associated steatotic liver disease (MASLD) constitutes 25% to 45% of chronic liver diseases [1], and its estimated prevalence worldwide increased to over 30% in 2019 reflecting the escalating obesity epidemic [2]. MASLD is a major contributing factor to chronic liver disorders. It consists of metabolic dysfunction-associated steatohepatitis (MASH) and metabolic dysfunction-associated steatotic liver (MASL). Conditions are characterized by lobular inflammation, hepatocyte ballooning, varying levels of pericellular fibrosis, and potential development of hepatocellular carcinoma [3].

MASLD is marked by a persistent injury to the parenchyma, involving repetitive phases of damage and recovery. Therefore, surgical excision remains one of the most potent curative therapeutic approaches for liver tumors; however, there is an increased risk of liver failure when hepatic steatosis is present [4]. Liver steatosis hinders ability to regenerate and compensate for lost volume after hepatectomy [5]. Some studies have suggested that presence of steatosis in patients prior to liver resection can lead to a growing risk of liver failure and postoperative complications following hepatectomy, which restricts surgical options in patients with fatty liver [6]. Thus, novel therapeutic means are needed to trigger a controlled regenerative response of the liver in this pathological condition.

Recent studies have shown that mitochondrial dysfunction is a key contributor to the initiation and progression of MASLD [7]. According to prior research, mitochondrial fatty acid oxidation (FAO) capacity and rate-limiting enzyme function in β -oxidation were reduced by roughly 40–50% in MASH patients compared to healthy individuals [8]. The mitochondrion plays a vital role in generating adenosine triphosphate (ATP) through oxidative phosphorylation and β -oxidation regulation, as well as producing ROS (reactive oxygen species) that cause cellular damage. Mitochondrial dysfunction leads to impaired ATP production, resulting in cellular functional impairment. Additionally, damaged mitochondria produce excessive ROS and thereby induce a negative spiral known as a “vicious cycle” [9]. Therefore, improving mitochondrial function is a promising approach for treatment of MASLD.

Mesenchymal stem cells (MSCs) demonstrate high proliferative capacity and self-renewal ability. These secrete

various growth factors to induce proliferation and differentiation of organ-constituent cells at the site of injury, thereby achieving organ function restoration [10]. MSCs also contribute to reducing inflammation by secreting various immunosuppressive and immune-regulatory factors [11]. Thus, due to their paracrine action and immunoregulatory function, MSCs have become a promising resource for cell transplantation. However, MSCs transplantation has limitations including low survival rate in vivo, depleted regenerative potential, and post-transplantation reduced cell differentiation.

It has been suggested that MSCs primarily exert their therapeutic effects through the secretion of trophic factors [12]. The MSCs culture media comprising the secretome is referred as MSCs conditioned medium (MSC-CM); it is considered a rich source of paracrine factors such as growth factors and cytokines [13]. Cell-free MSC-CM therapy confers key advantages over stem-cell based applications for important reasons. First, if administered intravascularly MSC-CM mitigates concerns with transplantation of living cells such as immune compatibility, tumorigenicity, and emboli formation. Second, MSC-CM is available in large-scale production and storage, so off-the-shelf therapy is feasible for treatment of acute clinical conditions. For these reasons, cell-free MSC-CM is a potential alternative to MSCs transplantation.

Meanwhile, hydrogels have received much attention in regenerative medicine, especially as a candidate drug delivery vehicle. Multiple reports have shown that hydrogel-encapsulated MSC-CM can continuously release growth factors and cytokines, which exerts pro-regenerative effects [14]. Although few studies have reported the intra-mesenteric space as an administration route for test drugs, systemic and splanchnic responses to intra-mesenteric and intravenous test drug were reported to be similar [15].

Some studies have demonstrated that MSCs transplantation and MSC-CM administration alleviate pathological changes in MASLD animal models [16, 17]. However, few studies have investigated effects of MSC-CM on regeneration after liver resection in MASLD. The aim of this study is to verify the therapeutic effect of MSC-CM on liver regeneration and explore its role in lipid metabolism after partial hepatectomy. To optimize utility of both MSC-CM and hydrogels, we administered MSC-CM encapsulated in hydrogel in the intra-mesenteric space of

the superior mesenteric vein (SMV) to support sustained delivery to remnant liver through the portal vein.

Methods

Animals

Six- to seven-week-old male Lewis rats were purchased from Charles River (Breeding Laboratories, Kanagawa, Japan). Rats were fed standard chow (CE-2; CLEA Japan Co., Ltd., Tokyo, Japan). All animals were maintained in a specific pathogen free animal facility at Jichi Medical University under a temperature- and humidity-controlled environment with alternating 12-h light/dark cycles with free access to food and water ad libitum. Animals received humane care which met the institutional guidelines for animal welfare. All experiments were conducted with approval from the Animal Care Committee of Jichi Medical University (approval number: 15–214) and performed in accordance with ARRIVE guidelines and the Japanese Guidelines for Animal Research.

Preparation of AT (adipose tissue derived) -MSC conditioned medium

The established method of rat AT-MSCs was described previously [18]. In brief, adipose tissue obtained from the inguinal region of wild-type LEW rat was minced into pieces. After shaking with an equal volume of PBS, the mixture was separated into two phases. The upper phase was digested with 0.075% collagenase (type 1) (Wako, Tokyo, Japan) in PBS for 1.5 h at 37 °C with shaking. The digested tissue was mixed with minimum essential medium α modification (MEM α ; Gibco-BRL, Tokyo, Japan), added with 10% fetal bovine serum (FBS; Gibco), and incubated for 10 min at room temperature. Subsequently, the lower phase was centrifuged and the resulting isolated AT-MSCs were seeded onto 100-mm tissue culture dishes (Thermo Scientific, Tokyo, Japan) cultured in MEM α supplemented with 10% FBS. AT-MSCs were cultured to reach confluence followed by a wash with PBS [–] and incubation in serum-free MEM α medium (GIBCO). After 2 days of culture, the supernatant was collected and then centrifuged, filtered, and concentrated at 12,000 rpm using Amicon Ultra centrifugal filters (Millipore, Tokyo, Japan; molecular weights 3, 10, 30, 50,

and 100 kDa). Liquids concentrated 1000-fold for each fraction's molecular weight were mixed to be utilized as MSC-CM in this study.

Characterization of rat AT-MSCs

The AT-MSCs at passage 5 were incubated with 10 μ L of Fc-blocker for 5 min and immunostained with Abs for 30 min at room temperature. After washing and labeling of dead cells with 7-AAD (Invitrogen), cells were analyzed using a FACSCalibur and CellQuest Pro Software (Becton Dickinson). AT-MSCs were stained with antibodies to CD29 (#102,207, BioLegend, San Diego, CA) CD31(#FAB3628G, R&D Systems, Minneapolis, MN), CD34 (sc-7324 AF647, Santa Cruz Biotechnology, Santa Cruz, CA), CD90 (#567,361, BioLegend) and CD105 (10,862–1-AP, Proteintech, Rosemont, IL) and their expressions were examined using FACSCalibur.

Trilineage differentiation of AT-MSCs

The differentiation potential of MSCs (passage 3) into adipocytes, osteocytes, or chondrocytes was evaluated using differentiation-induction media (PT-3002, PT-3003, PT-3004; Lonza, Basel, Switzerland) according to the manufacturer's protocols as previously described. After the specific differentiation culture, cells were analyzed by cytochemical staining with Oil Red-O, Alizarin Red, or Safranin-O, respectively.

Experimental protocol

We started feeding rats with a methionine and choline-deficient (MCD) diet (F2MCD; Oriental Yeast Co., Ltd., Tokyo, Japan) from 8 weeks old until the termination of experiment. After a MCD diet for 3 weeks, partial hepatectomy (PHx) was performed. During the surgical procedure, rats were allocated randomly into 2 groups: MSC-CM administered group and Control group (Fig. 1A). Animals were euthanized with an inhalation of excess isoflurane after the hepatectomy of 9 h, 30 h and 168 h. Blood samples were collected from the inferior vena cava for liver function tests and cytokine array analysis, and the liver was harvested and weighed. Standard diet-fed 11-week-old rats, and 11-week-old rats that had been fed an MCD diet for 3 weeks starting from 8 weeks

(See figure on next page.)

Fig. 1 Experimental protocol, characterization and tri-lineage differentiation of AT-MSCs and cytokine array analysis of MSC-CM. **A** After 3 weeks of MCD diet feeding, hepatectomy was performed. Rats were sacrificed at 9 h, 30 h and 168 h after hepatectomy. **B** Our model of 70% hepatectomy. **C** In the MSC-CM group, MSC-CM with peptide hydrogel as delivery vehicle was administered into the intra-mesenteric space of ileo-colic vein perfused area. In the control group, peptide hydrogel alone was administered. **D** Phase contrast images of rat AT-MSCs (original magnification, \times 100, scale bars represent 200 μ m). **E** Detection of rat AT-MSCs surface antigens by flow cytometry. AT-MSCs at passage 3–5 were stained with mAbs to CD29, CD31, CD34, CD105 and their expressions were examined. **F** AT-MSCs at passage 3 were induced to differentiate into adipocytes, osteoblasts, and chondrocytes-like cells (original magnification, \times 200, scale bars represent 100 μ m). **G** Images of cytokine array blots probed with MSC-CM used in this study

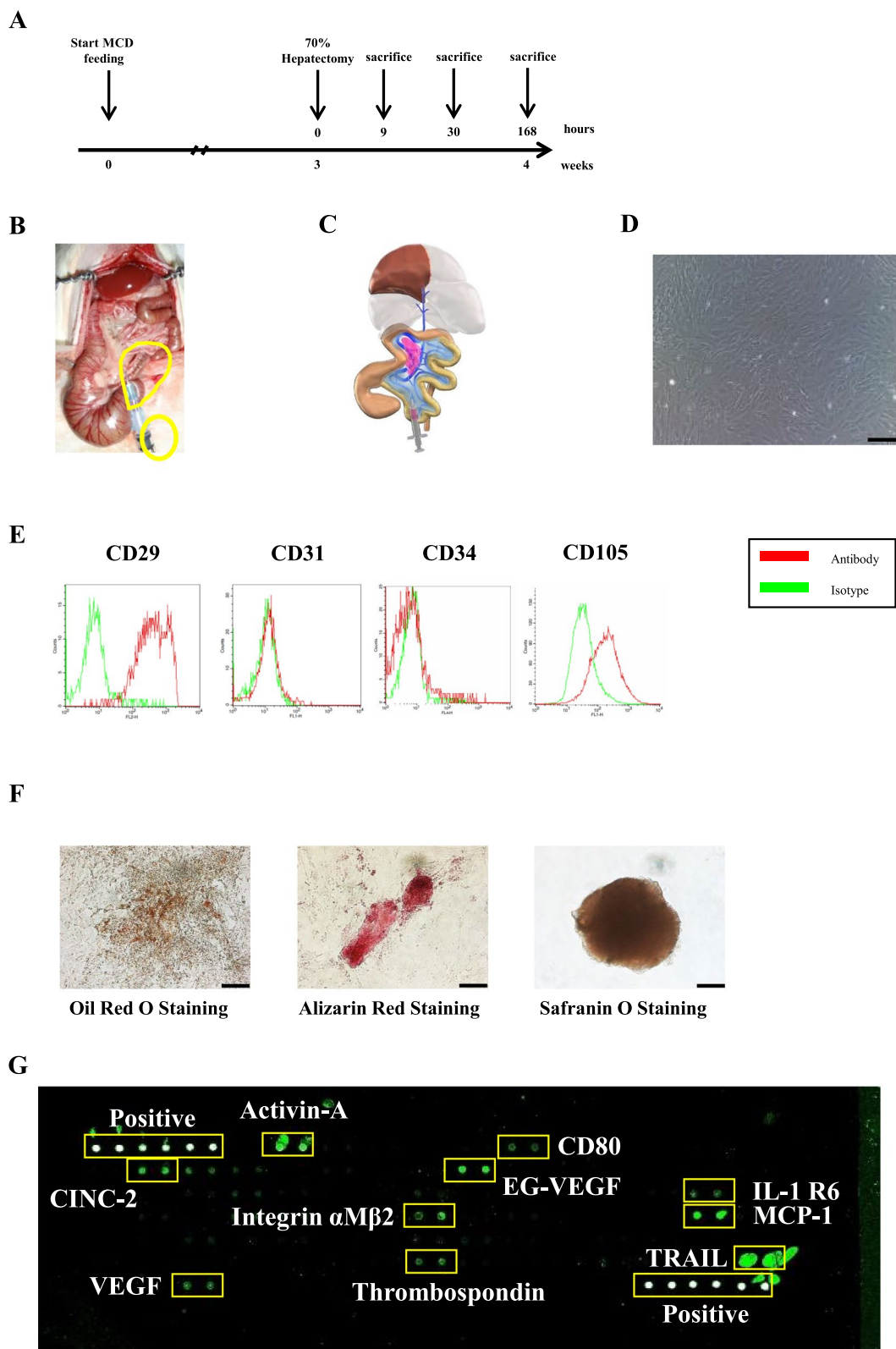


Fig. 1 (See legend on previous page.)

of age were euthanized to harvest liver tissues as specimens. Liver tissue samples were suitably stored for subsequent procedures.

Surgical procedure

Animals were fasted overnight and all procedures were performed under inhalation anesthesia using 1.5% isoflurane. After midventral laparotomy, the left lateral lobe, left portion of the medial lobe, right inferior superior lobes, and caudate lobes were resected with ligation of respective narrow pedicle using 4–0 silk, leaving only the medial lobe behind (Fig. 1B, C) as described previously [19]. Immediately after the hepatectomy, 1.0 ml of PuraMatrix™ (354,250, Corning, Corning, NY) was infused into the intra-mesenterium space of SMV perfused area with a 23-gauge needle followed by additional infusion of 100 µl of phosphate-buffered saline (PBS) or MSC-CM into the antecedently infused PuraMatrix™ (Fig. 1B, C), by which sustained release of MSC-CM to the liver via portal vein was feasible. The abdomen was closed with 4–0 nylon running sutures, and the rats were allowed to awaken from anesthesia.

Assessment of cytokines in MSC-CM

The cytokines in MSC-CM were measured using a biotin label-based rat antibody array (AAR-BLG and QAR-INF-1–1, Ray-Biotech, Norcross, GA). In brief, MSC-CM was dialyzed with dialysis buffer, labeled with biotin and incubated with arrays overnight at 4 °C. Glass slides were then incubated with Cy3-conjugated streptavidin overnight at 4 °C. Finally, the arrays were scanned and analyzed.

Assessment of liver function and serum cytokines

Blood samples were centrifuged for 10 min at 3000 rpm, and serum was collected. Serum alanine aminotransferase (ALT) was measured as an indicator of degrees of hepatocellular damage using a FUJIFILM DRI-CHEM 3500 machine (FujiFilm, Tokyo, Japan) and FUJI DRY CHEM SLIDES (FujiFilm) for GPT/alanine transaminase (ALT)-PIII. To assess the serum cytokines and chemokines, multiplexed sandwich ELISA-based quantitative array (QAR-CYT-3, Ray-Biotech) was used according to the manufacturer's directions (n=4 in each group at 9 h and 30 h after PHx). The arrays were scanned with GenePix® 4400A Microarray Scanner (Molecular Devices, Sunnyvale, CA), and images were analyzed using RayBio analysis tool.

Gene expression profiling

RNA was extracted from liver samples of rats 9 h after PHx, standard diet-fed rats without PHx (SD Hpx(-)), and MCD diet-fed rats without PHx (MCD Hpx(-)) (n=4/

group). Total RNA was extracted from frozen liver tissues using RNeasy Lipid Tissue Mini Kit (Qiagen) according to the manufacturer's instructions. The sense-strand DNA was amplified and then biotinylated according to the manufacturer's protocol from 250 ng total RNA (Expression Analysis WT Plus Technical Manual 2013; Affymetrix, Santa Clara, CA). Following fragmentation, the biotinylated sense-strand DNA underwent a 16-h hybridization at 45 °C on the GeneChip Rat Gene 2.0 ST Array. The GeneChips were washed and stained at the Affymetrix Fluidic Station 450, followed by scanning with the Affymetrix Gene Chip Scanner 3000 7G System. Affymetrix tools were used for preprocessing, and two algorithms designed to summarize microarray probes (robust multichip average algorithm and probe logarithmic intensity error) were implemented to enhance the statistical power in analyzing gene differentiation. For each probe set, gene and gene ontology annotations were established based on the annotation files available on the Affymetrix website (<http://www.affymetrix.com/>). Following thresholding and filtering, the log₂-normalized expression values were analyzed using a Database for Annotation, Visualization and Integrated Discovery (DAVID) and a comprehensive gene ontology (GO) term analysis.

Fisher's exact test was used to calculate a p-value determining the probability that the biological function assigned to that data set is explained by chance alone. The predicted activation state and activation z-scores were computed based on the direction of fold change values observed in the gene expression data.

Histological analysis

Liver tissues were fixed in 10% formalin for more than 24 h. Paraffin-embedded liver tissue Sects. (4 µm) were subjected to hematoxylin and eosin staining for histological analysis. Hepatocyte number per high-power field magnification (HPF 400X) was counted in 10 randomly selected fields per liver.

Immunohistochemical staining

After deparaffinization and rehydration, slides were treated with 3% hydrogen peroxide. Sections were subjected to antigen retrieval by heating to boiling in a 0.1 M Citrate Buffer Antigen Retrieval Solution (pH 6.0) for 20 min. To prevent non-specific binding of antibodies, sections were treated with 15% goat serum for 30 m. For immunohistochemical staining of PCNA, Ki-67, Cyclin D1, cleaved Caspase-3, and CD31, slides were then incubated with anti-PCNA antibody (sc-7907, Santa Cruz Biotechnology, Santa Cruz, CA), anti-Ki67 antibody (E1870, Spring Bioscience, Pleasanton, CA), anti-cyclin D1 antibody (sc-753, Santa Cruz Biotechnology),

anti-cleaved Caspase-3 antibody (#9664, Cell Signaling Technology, Danvers, MA), anti-CD31 antibody (ab182981, Abcam, Cambridge, UK), anti-CD163 antibody (sc-58965, Santa Cruz Biotechnology), and anti-E-cadherin antibody (20,874-1-AP, Proteintech) at 4°C overnight. The signal was detected with the ABC kit and DAB kit (Vector Laboratories, Burlingame, CA). Sections were counter-stained with hematoxylin. In morphometrical quantification of the staining area using Fiji/ImageJ (National Institutes of Health), all acquisition settings were the same for sections of both group within each immunostaining. Images were thresholded and quantified in Fiji/ImageJ software. The threshold within each set was kept constant for all images of both groups within a given confocal channel. Histological slides of the livers were analyzed in a blinded manner.

Identification of apoptotic hepatocytes

Three randomly selected HPF (200X) were selected to calculate the area stained by cleaved Caspase-3. The staining area was morphometrically quantified using Fiji/ImageJ (n=4–5/group). TUNEL assay was performed on 4- μ m liver sections using the FD Apop Kit (FD NeuroTechnologies, Columbia, MD) according to the manufacturer's instructions. The number of TUNEL-positive cells was counted from 10 randomly selected HPF (400X) per slides (n=4–5/group).

Liver regeneration rate

To estimate regeneration rate after partial hepatectomy, resected livers were weighed at time of procedure. The remnant liver was excised and weighed when the rats were sacrificed. Liver regeneration rates were calculated as the ratio of remnant liver weight/estimated whole liver weight. The original whole liver weight was extrapolated by calculating the resected liver weight/0.663, based on previous results [15].

Detection of proliferating hepatocytes

The number of PCNA-positive and Ki-67-positive cells per HPF was counted in 3 and 10 randomly selected fields per liver (n=4–5/group). Three HPF (200X) were randomly selected for calculating the staining area of the Cyclin D1. Mitosis per HPF (200X) was counted at 5 randomly selected fields per liver of anti-Cyclin D1 stained slide.

Measurement of hepatocyte size

Sections stained for E-cadherin were photographed at a magnification of 400X. The area of hepatocytes was measured by visualizing cell outlines through immunostaining with E-cadherin for 100 hepatocytes per rat using Fiji/ImageJ (n=4–5/group).

Evaluating damage to liver sinusoidal endothelial cells (SECs)

Evaluating damage to SECs was performed by immunohistochemical staining for CD31. To assess the stained area within the SECs, ten fields were selected randomly under high magnification (200X). The staining area was quantitatively analyzed using Fiji/ImageJ (n=4–5/group).

Morphometric Analysis of M2 macrophage populations

M2 Macrophage populations were analyzed on sections immunohistochemically stained for CD163 (M2 marker). Densities of M2 macrophages were analyzed on 5 fields at 200X on one representative slide. The mean densities were expressed as the number of positive cells per mm².

Measurement of liver lipid content

The measurement of triglyceride, total cholesterol, free cholesterol and phospholipid levels in rat livers using Folch's extraction procedure was outsourced to Immunobiological Laboratories Co., Ltd. (Fujioka, Japan).

Glycogen periodic acid Schiff stain

For periodic acid Schiff (PAS) stain, liver specimens were subjected to three 5-min PBS washes and then exposed to periodic acid for 8 min. Following two distilled water washes, staining with Schiff reagent was carried out for 20 min. After three distilled water rinses, specimens were treated with hematoxylin and inspected under a microscope. The staining area was quantitatively analyzed using Adobe Photoshop (n=4–5/group).

Quantification of liver ATP, β -hydroxybutyrate and acetyl CoA content

The hepatic ATP, β -hydroxybutyrate and acetyl CoA concentration were measured using an ATP Assay Kit (ab83355, Abcam), β -Hydroxybutyrate (Ketone Body) Fluorometric Assay Kit (700,740, Cayman Chemical, Ann Arbor, MI) and Acetyl CoA Assay Kit (ab87546, Abcam) according to manufacturer's instructions.

Statistical analysis

Prism software (GraphPad Software, Inc., La Jolla, CA) was used for statistical analyses. Data are presented as mean \pm SD. Student's *t*-test was used for comparison between groups, and *P*-values were used to quantify statistical significance (**P* < 0.05; ***P* < 0.01; ****P* < 0.001).

Results

The expression of the CD-surface markers in AT-MSCs

The AT-MSCs used in this study exhibited a fibroblastic morphology with a bipolar spindle shape (Fig. 1D). Flow cytometry immune profiling revealed positive expression for putative mesenchymal stem markers CD29 and

CD105. The endothelial marker CD31 and hematopoietic stem marker CD34 showed negative antigenic reactivity (Fig. 1E).

Tri-lineage differentiation capabilities of AT-MSCs

As functional MSCs, AT-MSCs should exhibit multi-lineage differentiation potential (adipogenic, osteogenic and chondrogenic) according to guideline recommendations of the International Society for Cellular Therapy (ISCT). We studied the tri-lineage differentiation potential of AT-MSCs. AT-MSCs demonstrated adipocyte, osteocyte and chondrocyte differentiation by Oil Red-O positive staining of lipid droplets, Alizarin Red staining of calcium deposits, and Safranin O staining of proteoglycan (Fig. 1F).

MSC-CM contained several kinds of cytokines including Activin-A and IL-10

The alignment of cytokine arrays is shown in Supplementary Table S1. Scanned image of cytokine array blots after incubation with MSC-CM are shown in Fig. 1G. The content of cytokines in MSC-CM were measured in a semiquantitative manner: Blots for TRAIL and Activin-A showed high signal intensity; MCP-1 and EG-VEGF showed moderate signal intensity; and CINC-2, Integrin α M β 2, VEGF, Thrombospondin, IL-1R6 and CD80 showed weak signal intensity. Next, content of inflammatory

cytokines in MSC-CM were measured in quantitatively (Table 1).

MSC-CM suppressed hepatectomy induced apoptosis

The serum ALT levels of the MSC-CM group at 9 h after hepatectomy were lower compared with those of the control group, although not significantly different ($P=0.07$, $n=4-5$ /group, Fig. 2A). To assess the effect of MSC-CM on apoptosis induced by hepatectomy, TUNEL analysis was performed on liver Sects. 9 h after hepatectomy. The number of apoptotic cells induced by hepatectomy in the MSC-CM group were significantly fewer compared with the control group ($P<0.01$, $n=4-5$ / group, Fig. 2B, C). Cleaved caspase-3 immunohistochemistry was performed and areas with relative cleaved caspase-3 positivity were examined to quantitatively evaluate the impact of MSC-CM on apoptosis. Relative cleaved caspase-3 positivity nuclei of MSC-CM group were significantly smaller than the control group ($P<0.01$, $n=4-5$ / group, Fig. 2D, E).

Serum levels of cytokines and chemokines at 9 h and 30 h after hepatectomy are shown in Fig. 3. Analyzed mediators are interleukin (IL) -2, IL-10, IL-13, fractalkine, tumor necrosis factor α (TNF- α), L-selectin, monocyte chemotactic protein 1 (MCP-1) and interferon γ (IFN- γ). The levels of serum of IL-2 and IL-10 were significantly higher in the MSC-CM group compared with controls ($P<0.05$, $n=4$ /group) at both 9 h and 30 h. The serum level of L-selectine was significantly higher in the MSC-CM group compared with controls ($P<0.05$, $n=4$ /group) at 9 h and the level of serum of IL-13, TNF- α , MCP-1 and IFN- γ were significantly higher in the MSC-CM group compared with controls ($P<0.01$ for MCP-1, $P<0.05$ for others, $n=4$ /group) at 30 h. However, the level of serum fractalkine was significantly higher at 9 h and significantly lower in the MSC-CM group compared with controls ($P<0.01$ for 9 h and $P<0.05$ for 30 h, $n=4$ /group).

MSC-CM promoted liver regeneration

All rats survived until sacrificed. The liver regeneration rates at 9 h, 30 h and 168 h after hepatectomy are shown in Fig. 4A. The liver regeneration rate was significantly higher in MSC-CM group at 30 h and 168 h compared to controls (at 30 h, regeneration rate of 49% vs. 44%, $P<0.05$, $n=4-5$ /group; at 168 h, 82% vs. 70%, $P<0.01$, $n=5-8$ /group). To investigate cell proliferation potential, PCNA expression which is a marker

Table 1 Content of inflammatory cytokines in MSC-CM used in the experiment

| Cytokine | Concentration (pg/ml) |
|---------------|-----------------------|
| IFN- γ | ND |
| IL-1 α | ND |
| IL-1 β | ND |
| IL-2 | 2243.1 |
| IL-4 | 18.0 |
| IL-6 | ND |
| IL-10 | 982.2 |
| IL-13 | ND |
| MCP-1 | 6396.7 |
| TNF α | ND |

ND not detected

(See figure on next page.)

Fig. 2 Assessments of apoptosis. **A** Serum ALT concentration at 9 h after hepatectomy. **B** Representative liver sections stained by TUNEL at 9 h after hepatectomy. Arrowheads indicate TUNEL positive nuclei of hepatocytes (original magnification, $\times 200$, scale bars represent 200 μ m). **C** Quantification of TUNEL-positive hepatocytes. **D** Quantification of cleaved Caspase-3 positive hepatocytes. **E** Representative liver sections stained by cleaved Caspase-3 at 9 h after hepatectomy (original magnification, $\times 200$, scale bars represent 200 μ m). Open bars, control group; closed bars, MSC-CM group. Data are presented as mean \pm SD ($*P<0.05$, $n=4-5$ /group)

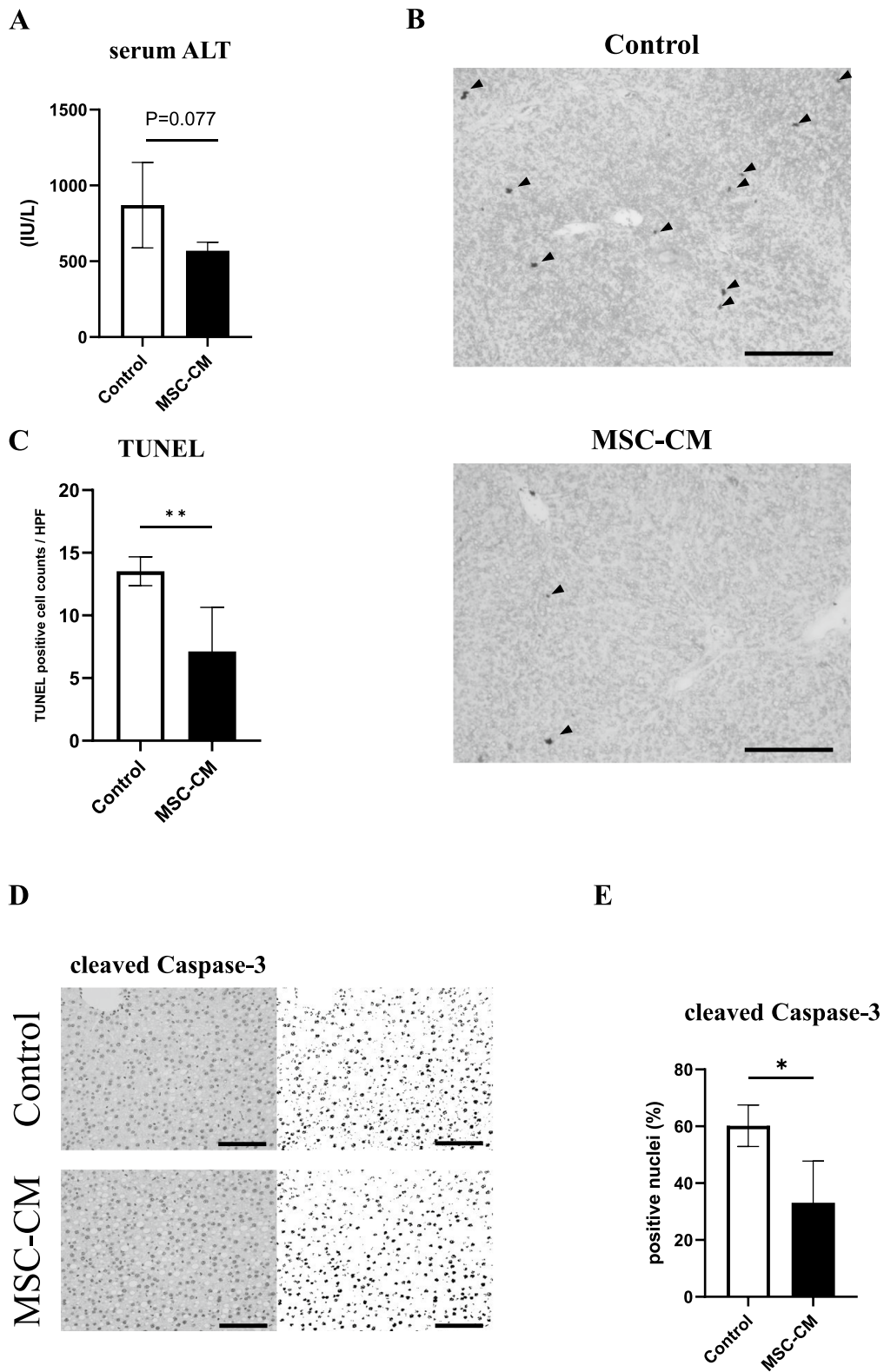


Fig. 2 (See legend on previous page.)

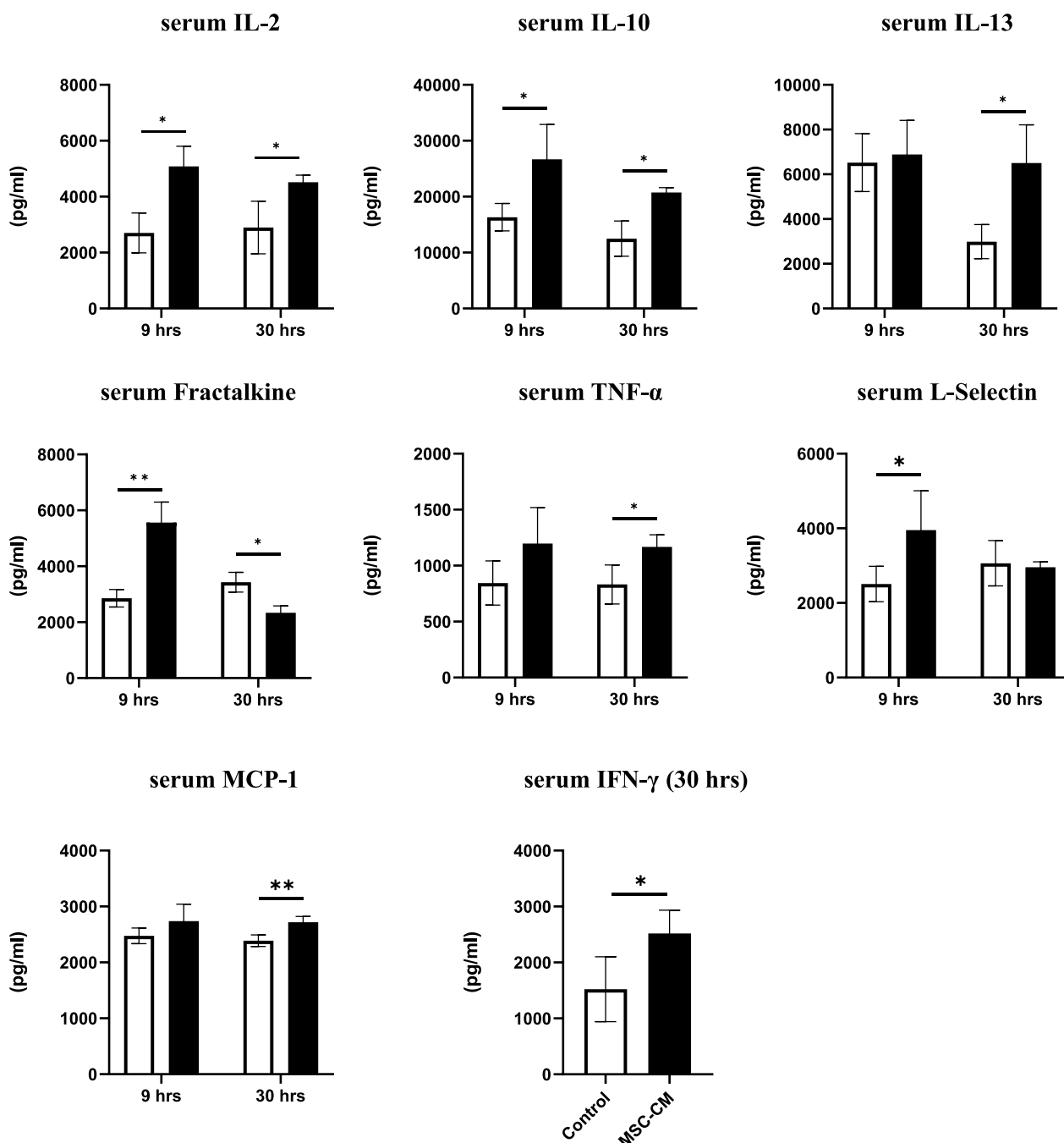


Fig. 3 Serum concentrations of cytokines and chemokines (IL-2, IL-10, IL-13, Fractalkine, TNF-α, L-Selectin, MCP-1) at 9 h and 30 h after hepatectomy. The data of IFN-γ is shown only those of at 30 h after hepatectomy. Open bars, control group; closed bars, MSC-CM group. Data are presented as mean ± SD (**P* < 0.05, ***P* < 0.01, *n* = 4/group)

of cell cycle entry and is elevated in the nucleus during late G1 phase and S phase, was assessed by immunostaining. The rate of PCNA-positive cells in the MSC-CM group was significantly higher at 30 h after hepatectomy compared with controls (*P* < 0.05, *n* = 4–5/group, Fig. 4B, D). Next, Ki-67 immunostaining was

performed. Unexpectedly, Ki-67 labeling index showed no significant difference between the groups (Fig. 4C, D).

Despite unaccompanied cell proliferation marker Ki-67 elevation, the liver regeneration rate was significantly higher at 30 h in the MSC-CM group. Thus, we

hypothesized that cell hypertrophy rather than cell proliferation contributed to liver regeneration in this model. To assess whether hepatocytes were enlarged, we measured the number of hepatocyte nuclei at 30 h after PHx in each liver section. The number of nuclei per field was significantly decreased in the MSC-CM group compared to controls ($P < 0.05$, $n = 4-5$ /group, Fig. 4E). Additionally, measurement of hepatocyte size revealed that hepatocyte size was significantly larger in the MSC-CM group versus controls ($P < 0.01$, $n = 4-5$ /group, Figs. 4F–H).

To evaluate MSC-CM effects on cell cycle during liver regeneration, CyclinD1 immunohistochemistry was performed and areas with relative CyclinD1 positivity were examined. Compared to controls, the MSC-CM group tended to have smaller CyclinD1 positive staining areas, but the difference was not statistically significant (Fig. 4I, J). We also assessed the number of mitotic figures in the same sections of CyclinD1 stain. The number of mitotic figures in MSC-CM group was significantly smaller than controls ($P < 0.001$, $n = 4-5$ /group, Fig. 4K, L).

Taken together, we confirmed presence of MSC-CM-induced hypertrophic proliferation with reductive cell division after PHx of MASLD liver. To assess angiogenesis during liver regeneration, sinusoidal endothelial cell staining was performed with CD31 antibody in liver sections at 30 h post-surgery. The CD31 positive area percentage was comparable between the groups (Supplementary Fig. S1). Next, to explore involvement of M2 macrophages in liver regeneration, staining of CD163-expressing macrophages was performed, but CD163-positive cell numbers were not significantly different between groups (Supplementary Fig. S2).

Changes in mRNA expressions in remnant liver by MSC-CM administration

To identify mechanisms by which MSC-CM promoted liver regeneration, we compared mRNA expressions at 9 h after PHx by microarray analysis. We hybridized 30,429 probe sets with amplified total RNA, filtering the raw data by removing entries not annotated with Symbol and Entrez ID, resulting in a total of 22,623 data points.

We evaluated the differentially expressed genes (DEGs) by performing three comparisons as follows: (1) MCD diet without PHx versus standard diet without PHx to identify the genes affected by MCD diet (Supplementary Table S2); (2) MCD diet with PHx (control group) versus MCD diet without PHx to detect the genes affected by PHx (Supplementary Table S3); (3) MCD diet with PHx and MSC-CM (MSC-CM group) versus MCD diet with PHx (control group) (Table 2) to analyze genes affected by administration of MSC-CM.

Using the combination of an FDR < 0.05 and a fold change > 2 as thresholds for statistical significance, 509 genes were found to be up- or down-regulated in MSC-CM group compared with controls, and top 10 DEGs in ascending order of FDRs are shown in Table 2. *RPS24.1* is an essential ribosomal protein for ribosome small subunit 40S, and *Rps25* is a part of cytosolic small ribosomal subunit. *RGDI561195* is known to be 60S ribosomal protein L31-like. Notably, the expression of *Mir770* was enhanced in controls compared to MCD diet without PHx (Supplementary Table S3), while it showed a decrease in the MSC-CM group compared to controls (Table 2). Studies have shown that an increase in *Mir770* expression leads to worsening diabetic nephropathy via apoptosis [20], while reducing *Mir770* expression results in decreased apoptosis in glioma cell lines [21]. By using the respective top-20 most significantly up- and down-regulated genes, hierarchical clustering analysis was performed to assess correlations and expression profiles of the DEGs. In the Fig. 5A, the genes are colored red and yellow. Among the 40 genes mentioned above, olfactory receptors (ORs) such as *Olr1448*, *Olr801*, *Olr1297*, *Olr1022*, *Olr1055*, *Olr1724* are included.

Subsequently, a volcano plot graph (Supplementary Fig. S3) was created to visualize significant DEGs. The scatter plot graph (Fig. 5B) shows distribution of significantly expressed mRNAs. To analyze potential functions and biological pathways of the DEGs further, GO enrichment analyses in the biological process (BP) was performed for compared groups according to the P -value. The predicted activation state and computed activation

(See figure on next page.)

Fig. 4 Assessments of liver regeneration. **A** Liver regeneration rates (%) at 9 h, 30 h, and 168 h after hepatectomy (9 h and 30 h: $n = 4-5$ /group, 168 h: $n = 5-8$ /group). **B** Quantification of PCNA-positive nuclei (%) at 30 h after hepatectomy ($n = 4-5$ /group). **C** Quantification of Ki-67-positive nuclei in both groups at 30 h after hepatectomy ($n = 4-5$ /group). **D** Representative immunohistochemical images from H&E, PCNA and Ki-67 at 30 h after hepatectomy (original magnification, $\times 400$; scale bars represent 100 μm). **E** The number of hepatocytes per HPF in the liver sections at 30 h after hepatectomy ($n = 4-5$ /group). **F** Hepatocyte size distribution. **G** Hepatocyte size in both groups. **H** Liver sections stained for E-cadherin are shown (original magnification, $\times 400$, scale bars represent 100 μm). **I** Representative liver sections stained by Cyclin D1 at 30 h after hepatectomy (original magnification, $\times 400$, scale bars represent 100 μm). **J** Relative Cyclin D1 positive area was morphologically quantified. **K** Representative liver sections stained by cyclin D1 at 30 h after hepatectomy. Arrows indicate mitotic figure in hepatocytes (original magnification, $\times 200$, scale bars represent 200 μm). **L** Quantification of mitotic figures in both groups. Open bars, control group; closed bars, MSC-CM group. Data are presented as mean \pm SD (* $P < 0.05$; ** $P < 0.01$; *** $P < 0.001$; $n = 4-5$ /group)

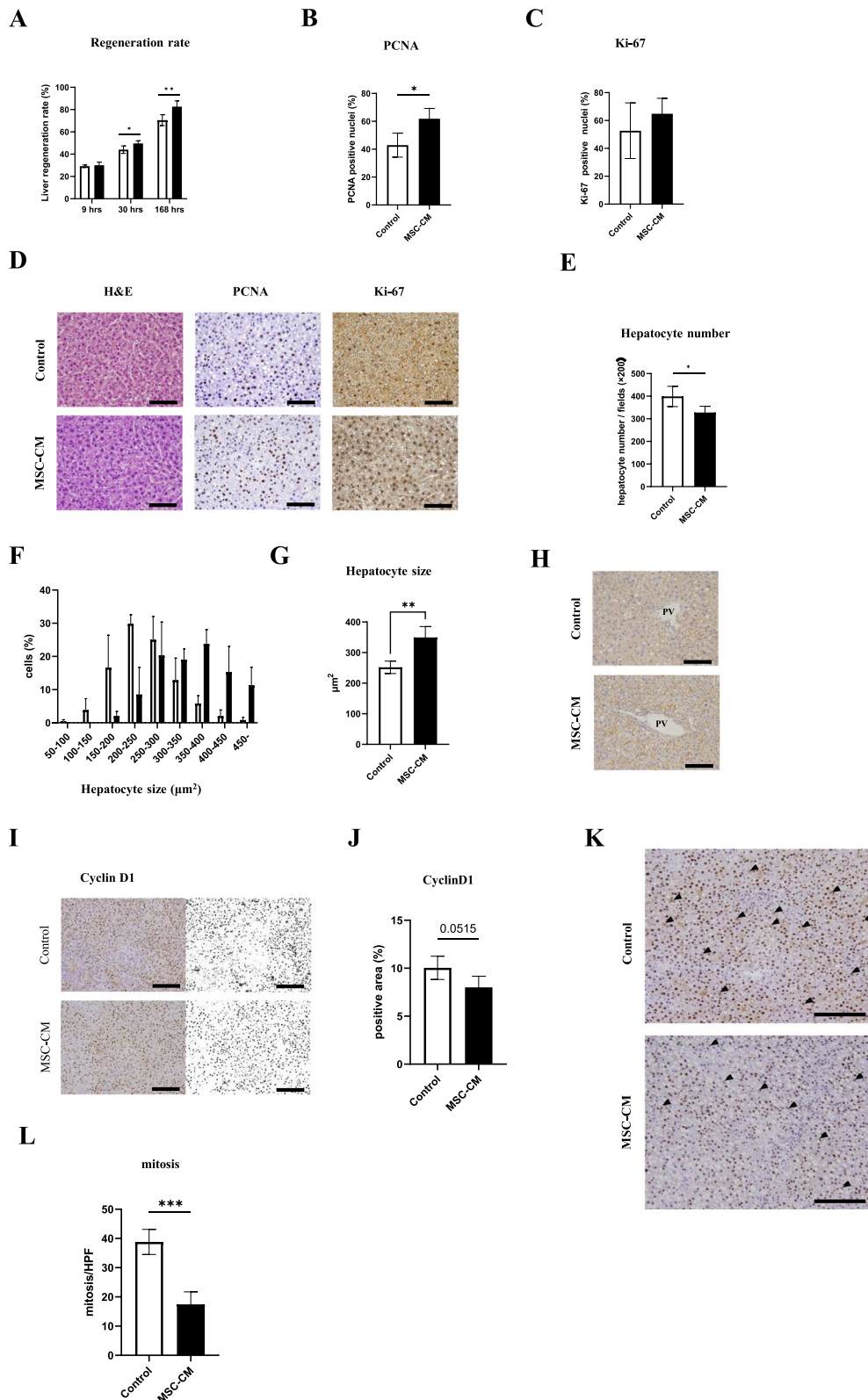


Fig. 4 (See legend on previous page.)

Table 2 Differential gene expression analysis of control group versus MSC-CM group at 9 h. Top 10 DEGs in ascending order of FDRs

| Symbol | logFC | logSIGNAL | P value | FDR |
|--------------|-------|-----------|-----------|-----------|
| RGD1563861 | 2.52 | 10.6 | 6.28E-180 | 1.42E-175 |
| RGD1311300.2 | -3.72 | 7.48 | 9.65E-63 | 1.09E-58 |
| Rbm25l1 | 1.69 | 8.51 | 2.84E-38 | 2.14E-34 |
| Rps24.1 | 2.76 | 7.00 | 2.97E-33 | 1.34E-29 |
| Rps25 | 2.76 | 7.00 | 2.97E-33 | 1.34E-29 |
| Timm23b | 1.13 | 9.38 | 6.84E-29 | 2.58E-25 |
| Cox7a2 | -3.84 | 6.13 | 2.32E-27 | 7.50E-24 |
| Mir770 | -0.90 | 10.1 | 2.72E-25 | 7.69E-22 |
| RGD1561195 | -1.82 | 7.54 | 3.08E-25 | 7.75E-22 |
| LOC501421.6 | -2.16 | 6.92 | 1.00E-22 | 2.06E-19 |

logFC \log_2 (average expression level of MSC-CM group) - \log_2 (average expression level of control group), *logSIGNAL* ($(\log_2$ (average expression level of Group control group) + \log_2 (average expression level of MSC-CM group)))/2, *P value* the p-value calculated by the exact test, the FDR (False Discovery Rate) calculated using the Benjamini-Hochberg method

z-score are based on the direction of fold change values in the gene expression data. The activation z-score infers probable states of activation, characterized as “increasing” or “decreasing”, and was considered significantly increased (or decreased) with an overlap p-value ≤ 0.05 and a z-score ≥ 2.0 (or ≤ -2.0) (Fig. 5C, Table 3). The down-regulated pathways included those related to G protein-coupled receptor signaling pathways, to detection of chemical stimulus involved in sensory perception of smell, and to sensory perception of smell and chemical stimulus, among others.

MSC-CM affected lipid metabolism and improved energetic status in remnant liver

To evaluate effects of MSC-CM on lipid metabolism in liver regeneration, we measured hepatic lipid content (Fig. 6A). Triglyceride (TG) content was significantly lower in the MSC-CM group compared to the control group. The free cholesterol (FC) content tended to decrease in the MSC-CM group compared to controls, although the difference was not significant. The content of total cholesterol (TC) and phospholipid (PL) showed no significant difference. Next, PAS staining was performed to assess glycogen storage in liver tissue. There was no significant difference in the PAS-positive area

between groups (Fig. 6B, C). To explore energetic status of the liver, hepatic content of ATP, β -hydroxybutyrate and Acetyl CoA at 168 h after PHx were measured. ATP and β -hydroxybutyrate content were significantly higher in the MSC-CM group compared to controls (Fig. 6D, E). In contrast, the MSC-CM group exhibited a significant decrease in acetyl CoA levels compared to the control group (Fig. 6F).

Discussion

Rats fed the MCD diet were used as a model of MASLD. The MCD diet induces systemic lipodystrophy that increases influx of free fatty acids to the liver, resulting in oxidative stress and hepatocyte apoptosis. Glucose storage was significantly reduced compared to standard diet-fed mice [22]. Here, mice with MASLD induced by a methionine-choline deficient diet had poorer post-surgical outcomes following hepatectomy compared to their healthier counterparts [23], reflecting the increased complications and death rates observed in MASLD patients undergoing partial hepatic resection [24].

In our study, administration of hydrogel-encapsulated MSC-CM to the intra-mesenteric space in rodent MASLD models significantly promoted liver regeneration after partial hepatectomy even until the termination stage of liver regeneration. Additionally, the mode of regeneration was dominated by cellular hypertrophy with a suppression of cell division. Furthermore, this regeneration was accompanied by maintenance of mitochondrial function, such as ATP production and β -oxidation of fatty acids, so energy produced in the mitochondria seemingly fueled liver regeneration.

Hepatocyte hypertrophic regeneration after partial hepatectomy has been thought to occur only when proliferative potential of hepatocytes is compromised, such as hepatocytes deficient in specific genes related to the cell cycle [25], bleeding [26] during hepatectomy, or administration of dexamethasone [27]. Interestingly, Miyaoka et al. reported that hypertrophy and proliferation almost equally contribute to liver regeneration after 70% partial hepatectomy in normal murine liver [28], which is contrary to proliferation dominantly contributing to regeneration.

Here, expression of cell cycle entry marker PCNA increased in the MSC-CM group compared to controls. In parallel, cyclin D1 expression and mitosis

(See figure on next page.)

Fig. 5 Differential expression analysis of liver tissue mRNA expression at 9 h for control group versus MSC-CM group. **A** Hierarchical clustering of four groups regarding the top 20 genes with the most significant fluctuations (standard diet-fed without PHx, MCD diet-fed without PHx, control group, MSC-CM group). **B** Scatter plots showing all the DEGs. **C** Bar chart of the most significant GO biological processes that are associated with up- and down-regulated genes. Red bars represent positive z-scores and blue bars indicate negative z-scores, with the color intensity reflecting the absolute magnitude of the z-score. X-axis represents the statistical significance of the enrichment ($-\log_{10}(p\text{-value})$)

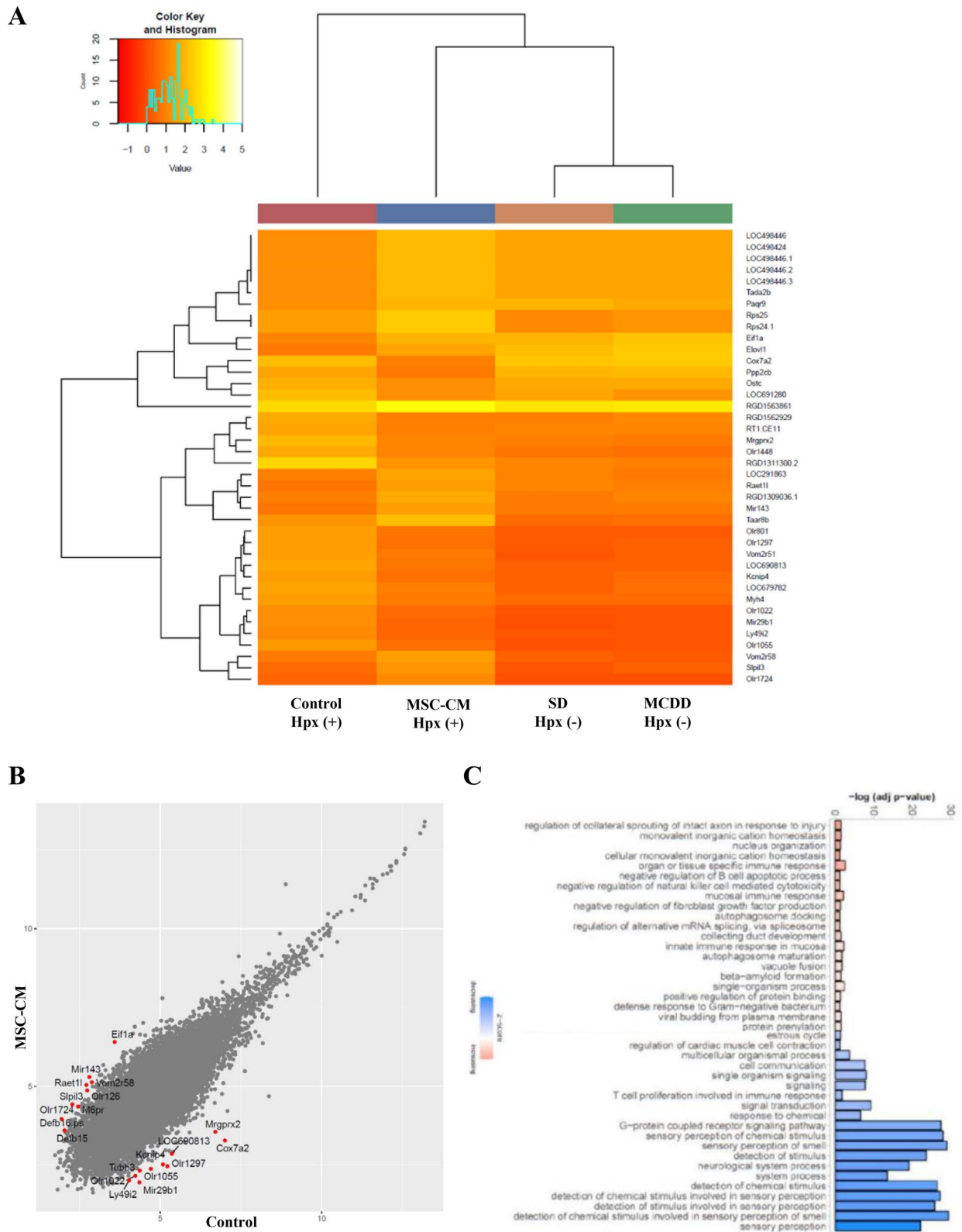


Fig. 5 (See legend on previous page.)

Table 3 GO Biological Processes that are enriched in DEGs in MSC-CM group compared with control group at 9 h. Top 10 GO biological processes in ascending order of *P* values

| GO.ID | Term | Annotated | Significant | Expected | <i>P</i> value |
|--------------|--|-----------|-------------|----------|----------------|
| GO:0007186 | G protein-coupled receptor signaling pathway | 981 | 155 | 107.11 | 9.00E-07 |
| GO:0050911 | Detection of chemical stimulus involved in sensory perception of smell | 75 | 21 | 8.19 | 3.50E-05 |
| GO:0002251 | Organ or tissue specific immune response | 45 | 14 | 4.91 | 0.0002 |
| GO:0002227 | Innate immune response in mucosa | 31 | 11 | 3.38 | 0.00027 |
| GO:0007608 | Sensory perception of smell | 110 | 25 | 12.01 | 0.00027 |
| GO:0007606 | Sensory perception of chemical stimulus | 262 | 47 | 28.61 | 0.00041 |
| GO:1,902,914 | Regulation of protein polyubiquitination | 28 | 10 | 3.06 | 0.00048 |
| GO:1,902,916 | Positive regulation of protein polyubiquitination | 16 | 7 | 1.75 | 0.00086 |
| GO:0019236 | Response to pheromone | 81 | 19 | 8.84 | 0.00095 |
| GO:0002385 | Mucosal immune response | 41 | 12 | 4.48 | 0.00106 |

were depressed in the MSC-CM group. The rate of Ki-67-positive nuclei was comparable between groups, suggesting no difference in proliferation. Concurrently, the liver regeneration rate was significantly increased in the MSC-CM group compared to controls at 30 h, which correspond to the progression/maintenance phase after hepatectomy. The above results indicate that MSC-CM-induced cell cycle arrest in fact *promoted* liver regeneration in a hepatocyte hypertrophic manner instead of hindering it.

Cytokine array analysis revealed that MSC-CM used in this study contained substantial amount of Activin-A. Activin-A plays the most crucial role in maintaining the homeostasis of liver weight. In a normal liver of quiescent state, moderate expression of Activin-A is observed. However, following partial hepatectomy, its expression dramatically decreases immediately. As regeneration progresses, its expression significantly increases, reaching its peak around when liver weight is restored to its original level [29]. Hepatocytes are the primary cells responsible for synthesis of Activin-A and exhibit a strong expression of type I and II activin receptors. Activin-A orchestrates inhibition of hepatocyte expansion via autocrine/paracrine pathways, highlighted by alterations in the expression of genes

governing proliferation and senescence, a reduced propensity for cell division [30].

Moreover, functional analysis identified that hepatocyte nuclear factor (HNF)-4 α might be critical targets of activin A signaling, implicating it in the regulation of hepatocyte proliferation and lipid homeostasis. Meanwhile activin-HNF4 α -coagulation axis plays a crucial role in determining clinical outcomes of severe acute liver failure [31]. Thus, Activin-A does not simply inhibit proliferation of hepatocytes but also promotes their survival and affects lipid metabolism, which aligns with this study's findings. To the best of our knowledge, effect of exogenous Activin-A administration after liver resection has not been reported previously. This unique pattern of hepatocyte hypertrophic regeneration demonstrated here through MSC-CM might be partially attributed to the action of Activin-A.

Previous research reported that impairments in oxidative phosphorylation such as decreased liver ATP synthesis increased production of ROS in MASH patients [32]. Therefore, mitochondrial dysfunction should play a significant role in the progression of MASH. Acetyl-CoA is normally generated through sugar and fatty acids (β -oxidation) metabolism and converts to ketone bodies in the liver under metabolic disturbances. Since

(See figure on next page.)

Fig. 6 Effect of MSC-CM on lipid metabolism and functional recovery after hepatectomy. **A** Liver tissue triglyceride (TG), total cholesterol (TC), phospholipids (PL), and free cholesterol content in livers at 168 h after hepatectomy ($n = 5-8$ /group). **B** Representative images of H&E (original magnification, $\times 400$, scale bars = 100 μm) and PAS ($\times 200$, scale bars = 200 μm) staining in liver slides at 168 h after hepatectomy. **C** Relative PAS staining positive area was morphologically quantified. **D** ATP concentrations in livers at 168 h after hepatectomy ($n = 5-8$ /group). For reference, values for both the standard diet-fed group (SD Hpx(-)) and the MCD diet-fed group without PHx (MCDD Hpx(-)) were also shown. **E** β -hydroxybutyrate concentrations in livers at 168 h after hepatectomy ($n = 5-8$ /group). Values for both the standard diet-fed group (SD Hpx(-)) and the MCD diet-fed group without PHx (MCDD Hpx(-)) were also shown. **F** Acetyl CoA concentrations in livers at 168 h after hepatectomy ($n = 5-8$ /group). Open bars, control group; closed bars, MSC-CM group; dark gray bars, MCDD Hpx(-) group; light gray bars, SD Hpx(-) group. Data are presented as mean \pm SD (** $P < 0.05$, *** $P < 0.001$, $n = 5-8$ /group)

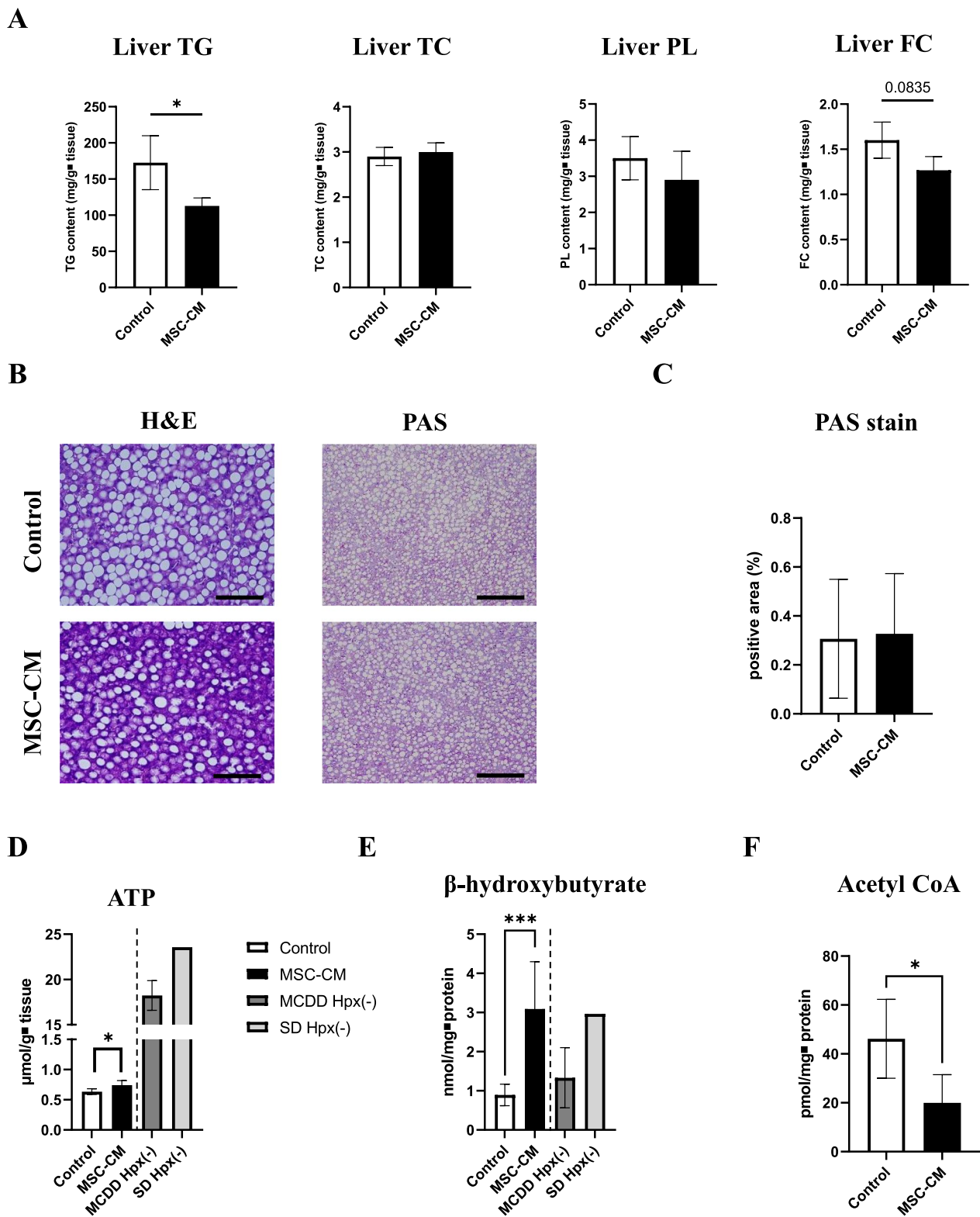


Fig. 6 (See legend on previous page.)

acetyl-CoA produces ATP in the tricarboxylic acid (TCA) cycle, energy shortage occurs due to defective utilization of acetyl-CoA in starvation state and thereby enhancement of β -oxidation to generate ketone bodies is required. Intrahepatic glycogen and free glucose storage were significantly reduced in mice fed the MCD diet [33], indicating that supply shortage and impaired utilization of acetyl-CoA coexist in this animal model of MCD diet-induced MASLD-like features in the context of leanness, leading to ATP deficit in liver.

Analogous to our results, reduction in phosphatase and tensin homolog (PTEN) expression following hepatectomy enhances utilization of transient regeneration-associated steatosis (TRAS)-derived accumulated liver lipids by β -oxidation in mitochondria [34], providing energy for hypertrophic liver regeneration. Our results demonstrated that MSC-CM treatment improved liver regeneration rate as well as increased ATP and β -hydroxybutyrate content and decreased acetyl CoA and triglyceride in remnant liver until the termination phase of regeneration after hepatectomy. This implies that MSC-CM promoted liver regeneration not only in liver volume, but also in functionality by affecting lipid metabolism as fuel sources to support regeneration. Further studies are needed to clarify the functional link among MSC-CM, hepatocyte hypertrophic regeneration and β -oxidation.

This study also showed that the serum levels of IL-10 at 9 h and 30 h after hepatectomy were significantly higher in the MSC-CM group. IL-10 is a cytokine with anti-inflammatory properties that plays a pivotal role in modulating immune responses. It is produced by almost all subsets of leukocytes, including dendritic cells, macrophages, T cells, natural killer cells, B cells [35] and MSCs. IL-10 secreted by transplanted MSCs activated the mammalian target of rapamycin (mTOR) pathway and thereby enhanced mitochondrial function as well as correct abnormal lipid metabolism in treating post-hepatectomy liver failure [36]. Although MSC-CM used in our model contained IL-10, its concentration was not high compared to serum IL-10 levels. It is possible that the other factors in MSC-CM acted on IL-10 producing cells to enhance IL-10 production.

Olfactory receptors (ORs) are seven-transmembrane G protein-coupled receptors (GPCRs) located mainly in olfactory sensory neurons of the olfactory epithelium. GPCRs play a crucial role as chemosensors by detecting and decoding chemical signals in their environment [37]. ORs are ectopically expressed throughout the body including liver [38], heart [39], kidney [40], and pancreas [41]. The liver is the largest metabolic organ regulating whole-body homeostasis by sensing and detoxifying drugs, alcohol, and environmental toxins, metabolizing nutrients, synthesizing and secreting bile acids, and

removing toxins and other waste products from the blood. Thus, the liver appears to be primed to utilize these ORs.

Recently, several groups have identified distinctive metabolic functions for hepatic ORs. *Olfir734* responds to Asprosin and serves as a fasting-induced glucogenic hormone [42]. Asprosin is encoded by *FBNI* gene whose mRNA expression is confirmed to be abundant in MSCs. In addition, *Olfir544* can trigger lipolysis upon activation in diabetic mice [43]. Notably, GO enrichment analysis showed that expression of functional category sensory perception of smell genes were enhanced following hepatectomy (the control group) compared with the MCD-fed alone group, whereas those genes were suppressed in the MSC-CM group compared with the control group. For the brain to identify a wide variety of odors, it is crucial that each sensor carries only one type of olfactory receptor, a principle known as the 'one sensor, one receptor' rule. Once a specific set of ORs is activated, inhibiting activation of other OR genes in that cell becomes necessary. This is ensured by a negative feedback mechanism deactivating additional specific control regions known as locus control regions and their associated protein factors, thereby upholding the principle of one neuron per receptor [44].

This led us to speculate that MSC-CM might contain factors serving as ligands for certain olfactory receptors, and their delivery subsequently suppressed expression of other olfactory gene receptors. ORs in the liver could potentially function as chemical sensors, altering liver metabolism. Further detailed research is necessary to determine whether MSC-CM contains ligands for specific ORs, and the impact of activating those ORs on liver regeneration.

Pharmacological alteration of macrophage polarization towards an M2 phenotype has been shown to partially reverse liver steatosis [45]. Moreover, in animal models of acute liver failure (ALF), MCP-1 and Siglec-9 secreted from human exfoliated deciduous tooth-derived mesenchymal stem cells have been shown synergistically to promote the M2 differentiation of bone marrow-derived macrophages via CCR2 and thereby improved the survival of ALF rats [46]. In our model, MSC-CM containing certain amounts of MCP-1 did not alter the number of CD163-positive cells, a specific marker of M2-type macrophage, implying that regeneration effect of MSC-CM was not M2-type macrophage-mediated.

In liver regeneration after partial hepatectomy, vascular remodeling through autocrine and paracrine control mediated by angiogenic growth factors and their receptors is known to be involved. Hepatocyte produce VEGF within 48 h-72 h after PHx, promoting sinusoidal endothelial cell proliferation and

hepatocyte proliferation [47]. Additionally, VEGF promotes hepatocyte proliferation by inducing HGF production through VEGFR1 in LSECs [48]. The MSC-CM here contained certain amount of VEGF, so we assessed angiogenesis during regeneration by CD31 immunohistochemistry. Unexpectedly, results revealed that MSC-CM did not seem to affect angiogenesis in this model.

Various differences in liver metabolic functions between humans and experimental animals such as mice and rats have been reported. Recent studies have shown that human liver organoids can replicate inflammation and fibrosis in MASLD [49, 50]. To determine whether our findings can be applied to human clinical practice, future research should investigate the effects of human MSC-CM on post-hepatectomy liver regeneration with MASLD as background liver disease in an *in vitro* model using human liver organoids.

Conclusions

Delivering MSC-CM encapsulated hydrogel to intra-mesenteric space in a controlled-release manner during hepatectomy for MASLD patients might be a feasible and safe approach, potentially serving as an attractive therapeutic modality that supports the reduction of post-surgical complications and death rates.

Abbreviations

| | |
|----------------|---|
| 7-AAD | 7-Amino-actinomycin D |
| ALT | Alanine transaminase |
| ATP | Adenosine triphosphate |
| DAVID | Database for annotation, visualization and integrated discovery |
| FAO | Fatty acid beta-oxidation |
| FC | Free cholesterol |
| GO | Gene ontology |
| GPCRs | G protein-coupled receptors |
| HNF-4 α | Hepatocyte nuclear factor-4 α |
| IFN- γ | Interferon- γ |
| MASH | Metabolic dysfunction-associated steatohepatitis |
| MASLD | Metabolic dysfunction-associated steatotic liver disease |
| MCD | Methionine and choline-deficient |
| MCP-1 | Monocyte chemoattractant protein-1 |
| MSCs | Mesenchymal stem cells |
| MSC-CM | MSCs conditioned medium |
| mTOR | Mammalian target of rapamycin |
| ORs | Olfactory receptors |
| PAS | Periodic acid-Schiff |
| PCNA | Proliferating cell nuclear antigen |
| PHx | Partial hepatectomy |
| PL | Phospholipid |
| PTEN | Phosphatase and tensin homolog |
| ROS | Reactive oxygen species |
| SECs | Sinusoidal endothelial cells |
| TC | Total cholesterol |
| TCA | Tricarboxylic acid |
| TG | Triglyceride |
| TNF- α | Tumor necrosis factor- α |
| TRAS | Transient regeneration-associated steatosis |
| TUNEL | TdT-mediated dUTP Nick-end labeling |

Supplementary Information

The online version contains supplementary material available at <https://doi.org/10.1186/s13287-024-03993-w>.

Additional file 1

Acknowledgements

The authors thank Dr. K. Fukuda, Ms. K. Tsujikado, Ms. A. Takei, Mr. K. Hayashi, and Ms. A. Ono from the Cooperative Research Center of Dokkyo Medical University Saitama Medical Center. The authors also thank Dr. Adam Lebowitz for editing a draft of this manuscript.

Author contributions

N.K. and T.T. contributed to the conceptualization. S.Y. and Y.S. contributed to the formal analysis. N.K., T.T., Y.K., K.S., H.S., Y.F. and T.U. contributed to the investigation. T.T. and H.O. contributed to the resources. T.T. contributed to the supervision. N.K. contributed to the writing—original draft. S.Y., H.Y., J.K. and N.S. contributed to the writing—review and editing. All authors reviewed the manuscript.

Funding

This work was supported by JSPS KAKENHI Grant Numbers JP26461926 (to NK) and JP17K10563 (to NK) and by a Jichi Medical University Young Investigator Award (to NK).

Availability of data and materials

All data generated or analyzed during this study were included in this published article and its supplementary information files.

Declarations

Ethic approval and consent to participate

(1) All experiments were conducted with approval. Title of the approved project: The investigation of the therapeutic effects of MSC-secreted factors on NASH using a rodent model. (2) Name of the institutional approval committee or unit: The Animal Care Committee of Jichi Medical University. (3) Approval number: 15-214. (4) Date of approval: April 1st, 2016. We did not use any human cells/ cell-lines/ samples in the present study.

Competing interests

The author(s) declare no competing interests.

Consent for publication

Not applicable.

Author details

¹Department of Surgery, Jichi Medical University, Shimotsuke, Japan. ²Division of Translational Research, Jichi Medical University, Shimotsuke, Japan. ³Department of Surgery, Japanese Red Cross Otsu Hospital, Otsu, Japan. ⁴Department of Transplant Surgery, Nagoya University Hospital, Nagoya, Japan. ⁵Department of Surgery, Dokkyo Medical University Saitama Medical Center, Koshigaya, Japan.

Received: 4 May 2024 Accepted: 10 October 2024

Published online: 04 November 2024

References

- Rinella ME. Nonalcoholic fatty liver disease: a systematic review. *JAMA*. 2015;313:2263–73.
- Henry L, Paik J, Younossi ZM. Review article: the epidemiologic burden of non-alcoholic fatty liver disease across the world. *Aliment Pharmacol Ther*. 2022;56:942–56.
- Cotter TG, Rinella M. Nonalcoholic fatty liver disease 2020: the state of the disease. *Gastroenterology*. 2020;158:1851–64.

4. Colle I, Verhelst X, Vanlander A, Geerts A, Van Vlierberghe H, Berrevoet F, Rogiers X, Troisi RI. Pathophysiology and management of post resection liver failure. *Acta Chir Belg*. 2013;113:155–61.
5. Kele PG, van der Jagt EJ, Gouw AS, Lisman T, Porte RJ, de Boer MT. The impact of hepatic steatosis on liver regeneration after partial hepatectomy. *Liver Int*. 2013;33:469–75.
6. van Keulen AM, Olthof PB, Buettner S, Bednarsch J, Verheij J, Erdmann JI, Nooijen LE, Porte RJ, Minnee RC, Murad SD, Neumann UP, Heijl L, Groot Koerkamp B, Doukas M. The influence of hepatic steatosis and fibrosis on postoperative outcomes after major liver resection of perihilar cholangiocarcinoma. *Ann Surg Oncol*. 2024;31:133–41.
7. Mansouri A, Gattoliat CH, Asselah T. Mitochondrial dysfunction and signaling in chronic liver diseases. *Gastroenterology*. 2018;155:629–47.
8. Moore MP, Cunningham RP, Meers GM, Johnson SA, Wheeler AA, Ganga RR, Spencer NM, Pitt JB, Diaz-Arias A, Swi AIA, Hammoud GM, Ibdah JA, Parks EJ, Rector RS. Compromised hepatic mitochondrial fatty acid oxidation and reduced markers of mitochondrial turnover in human NAFLD. *Hepatology*. 2022;76:1452–65.
9. Loria P, Lonardo A, Anania F. Liver and diabetes A vicious circle. *Hepatol Res*. 2013;43:51–64.
10. Andrzejewska A, Lukomska B, Janowski M. Concise review: mesenchymal stem cells: from roots to boost. *Stem Cells*. 2019;37:855–64.
11. Shi Y, Wang Y, Li Q, Liu K, Hou J, Shao C, Wang Y. Immunoregulatory mechanisms of mesenchymal stem and stromal cells in inflammatory diseases. *Nat Rev Nephrol*. 2018;14:493–507.
12. Wang J, Cen P, Chen J, Fan L, Li J, Cao H, Li L. Role of mesenchymal stem cells, their derived factors, and extracellular vesicles in liver failure. *Stem Cell Res Ther*. 2017;8:137.
13. L PK, Kandoi S, Misra R, S V, K R, Verma RS. The mesenchymal stem cell secretome: A new paradigm towards cell-free therapeutic mode in regenerative medicine. *Cytokine Growth Factor Rev*. 2019; 46:1–9.
14. Huang Y, Li X, Yang L. Hydrogel encapsulation: taking the therapy of mesenchymal stem cells and their derived secretome to the next level. *Front Bioeng Biotechnol*. 2022;10:859927.
15. Colle I, De Vriese AS, Van Vlierberghe H, Lameire NH, DeVos M. Systemic and splanchnic haemodynamic effects of sildenafil in an in vivo animal model of cirrhosis support for a risk in cirrhotic patients. *Liver Int*. 2004;24:63–8.
16. Lee CW, Hsiao WT, Lee OK. Mesenchymal stromal cell-based therapies reduce obesity and metabolic syndromes induced by a high-fat diet. *Transl Res*. 2017;182:61–74.e8.
17. Yang M, Cui Y, Song J, Cui C, Wang L, Liang K, Wang C, Sha S, He Q, Hu H, Guo X, Zang N, Sun L, Chen L. Mesenchymal stem cell-conditioned medium improved mitochondrial function and alleviated inflammation and apoptosis in non-alcoholic fatty liver disease by regulating SIRT1. *Biochem Biophys Res Commun*. 2021;546:74–82.
18. Teratani T, Kasahara N, Fujimoto Y, Sakuma Y, Miki A, Goto M, Sata N, Kitayama J. Mesenchymal stem cells secretions enhanced ATP generation on isolated islets during transplantation. *Islets*. 2022;14:69–81.
19. Kanazawa H, Fujimoto Y, Teratani T, Iwasaki J, Kasahara N, Negishi K, Tsuruyama T, Uemoto S, Kobayashi E. Bone marrow-derived mesenchymal stem cells ameliorate hepatic ischemia reperfusion injury in a rat model. *PLoS ONE*. 2011;6:e19195.
20. Zhang J, Song L, Ma Y, Yin Y, Liu X, Luo X, Sun J, Wang L. IncRNA MEG8 upregulates miR-770-5p through methylation and promotes cell apoptosis in diabetic nephropathy. *Diabetes Metab Syndr Obes*. 2020;13:2477–83.
21. Zhang JF, Zhang JS, Zhao ZH, Yang PB, Ji SF, Li N, Shi QD, Tan J, Xu X, Xu CB, Zhao LY. MicroRNA-770 affects proliferation and cell cycle transition by directly targeting CDK8 in glioma. *Cancer Cell Int*. 2018;18:195.
22. Fisher FM, Chui PC, Nasser IA, Popov Y, Cunniff JC, Lundasen T, Khari-tonenkova A, Schuppan D, Flier JS, Maratos-Flier E. Fibroblast growth factor 21 limits lipotoxicity by promoting hepatic fatty acid activation in mice on methionine and choline-deficient diets. *Gastroenterology*. 2014;147:1073–83.e6.
23. van den Broek MA, Olde Damink SW, Dejong CH, Lang H, Malagó M, Jalan R, Saner FH. Liver failure after partial hepatic resection: definition, pathophysiology, risk factors and treatment. *Liver Int*. 2008;28(6):767–80. <https://doi.org/10.1111/j.1478-3231.2008.01777.x>.
24. de Meijer VE, Kalish BT, Puder M, Ijzermans JN. Systematic review and meta-analysis of steatosis as a risk factor in major hepatic resection. *Br J Surg*. 2010;97(9):1331–9. <https://doi.org/10.1002/bjs.7194>.
25. Haga S, Ogawa W, Inoue H, Terui K, Ogino T, Igarashi R, Takeda K, Akira S, Enosawa S, Furukawa H, Todo S, Ozaki M. Compensatory recovery of liver mass by Akt-mediated hepatocellular hypertrophy in liver-specific STAT3-deficient mice. *J Hepatol*. 2005;43:799–807.
26. Matot I, Nachmansson N, Duev O, Schulz S, Schroeder-Stein K, Frede S, Abramovitch R. Impaired liver regeneration after hepatectomy and bleeding is associated with a shift from hepatocyte proliferation to hypertrophy. *FASEB J*. 2017;31:5283–95.
27. Nagy P, Teramoto T, Factor VM, Sanchez A, Schnur J, Paku S, Thorgeirsson SS. Reconstitution of liver mass via cellular hypertrophy in the rat. *Hepatology*. 2001;33:339–45.
28. Miyaoka Y, Ebato K, Kato H, Arakawa S, Shimizu S, Miyajima A. Hypertrophy and unconventional cell division of hepatocytes underlie liver regeneration. *Curr Biol*. 2012;22:1166–75.
29. Endo D, Maku-Uchi M, Kojima I. Activin or follistatin: which is more beneficial to support liver regeneration after massive hepatectomy? *Endocr J*. 2006;53:73–8.
30. Haridoss S, Yovchev MI, Schweizer H, Megherhi S, Beecher M, Locker J, Oertel M. Activin A is a prominent autocrine regulator of hepatocyte growth arrest. *Hepatol Commun*. 2017;1:852–70.
31. Lin T, Wang S, Munker S, Jung K, Macías-Rodríguez RU, Ruiz-Margáin A, Schierwagen R, Liu H, Shao C, Fan C, Feng R, Yuan X, Wang S, Wandrer F, Meyer C, Wimmer R, Liebe R, Kroll J, Zhang L, Schiergens T, Ten Dijke P, Teufel A, Marx A, Mertens PR, Wang H, Ebert MPA, Bantel H, Toni E, Trebicka J, Dooley S, Shin D, Ding H, Weng HL. Follistatin-controlled activin-HNF4 α -coagulation factor axis in liver progenitor cells determines outcome of acute liver failure. *Hepatology*. 2022;75:322–37.
32. Pérez-Carreras M, Del Hoyo P, Martín MA, Castro JC, Martín A, Castellano G, Colina F, Arenas J, Solís-Herruzo JA. Defective hepatic mitochondrial respiratory chain in patients with nonalcoholic steatohepatitis. *Hepatology*. 2003;38:999–1007.
33. Valdecantos MP, Pardo V, Ruiz L, Castro-Sánchez L, Lanzón B, Fernández-Millán E, García-Monzón C, Arroba AI, González-Rodríguez Á, Escrivá F, Álvarez C, Rupérez FJ, Barbas C, Konkar A, Naylor J, Hornigold D, Santos AD, Bednarek M, Grimsby J, Rondinone CM, Valverde ÁM. A novel glucagon-like peptide 1/glucagon receptor dual agonist improves steatohepatitis and liver regeneration in mice. *Hepatology*. 2017;65:950–68.
34. Kachaylo E, Tschuor C, Calo N, Borgeaud N, Ungethüm U, Limani P, Piquet AC, Dufour JF, Foti M, Graf R, Clavien PA, Humar B. PTEN Down-regulation promotes β -oxidation to fuel hypertrophic liver growth after hepatectomy in mice. *Hepatology*. 2017;66:908–21.
35. Ip WKE, Hoshi N, Shouval DS, Snapper S, Medzhitov R. Anti-inflammatory effect of IL-10 mediated by metabolic reprogramming of macrophages. *Science*. 2017;356:513–9.
36. Wang JL, Ding HR, Pan CY, Shi XL, Ren HZ. Mesenchymal stem cells ameliorate lipid metabolism through reducing mitochondrial damage of hepatocytes in the treatment of post-hepatectomy liver failure. *Cell Death Dis*. 2021;12:111.
37. Manzini I, Schild D, Di Natale C. Principles of odor coding in vertebrates and artificial chemosensory systems. *Physiol Rev*. 2022;102:61–154.
38. Kurtz R, Steinberg LG, Betcher M, Fowler D, Shepard BD. The sensing liver: localization and ligands for hepatic murine olfactory and taste receptors. *Front Physiol*. 2020;11:574082.
39. Kim SH, Yoon YC, Lee AS, Kang N, Koo J, Rhyu MR, Park JH. Expression of human olfactory receptor 10J5 in heart aorta, coronary artery, and endothelial cells and its functional role in angiogenesis. *Biochem Biophys Res Commun*. 2015;460:404–8.
40. Rajkumar P, Aisenberg WH, Acres OW, Protzko RJ, Pluznick JL. Identification and characterization of novel renal sensory receptors. *PLoS ONE*. 2014;9:e111053.
41. Kang N, Bahk YY, Lee N, Jae Y, Cho YH, Ku CR, Byun Y, Lee EJ, Kim MS, Koo J. Olfactory receptor Olfr544 responding to azelaic acid regulates glucagon secretion in α -cells of mouse pancreatic islets. *Biochem Biophys Res Commun*. 2015;460:616–21.
42. Li E, Shan H, Chen L, Long A, Zhang Y, Liu Y, Jia L, Wei F, Han J, Li T, Liu X, Deng H, Wang Y. OLF734 mediates glucose metabolism as a receptor of asprosin. *Cell Metab*. 2019;30:319–28.

43. Wu C, Hwang SH, Jia Y, Choi J, Kim YJ, Choi D, Pathiraja D, Choi IG, Koo SH, Lee SJ. Olfactory receptor 544 reduces adiposity by steering fuel preference toward fats. *J Clin Invest*. 2017;127:4118–23.
44. Serizawa S, Miyamichi K, Nakatani H, Suzuki M, Saito M, Yoshihara Y, Sakano H. Negative feedback regulation ensures the one receptor-one olfactory neuron rule in mouse. *Science*. 2003;302:2088–94.
45. Luo W, Xu Q, Wang Q, Wu H, Hua J. Effect of modulation of PPAR- γ activity on Kupffer cells M1/M2 polarization in the development of non-alcoholic fatty liver disease. *Sci Rep*. 2017;7:44612.
46. Ito T, Ishigami M, Matsushita Y, Hirata M, Matsubara K, Ishikawa T, Hibi H, Ueda M, Hirooka Y, Goto H, Yamamoto A. Secreted Ectodomain of SIGLEC-9 and MCP-1 synergistically improve acute liver failure in rats by altering macrophage polarity. *Sci Rep*. 2017;7:44043.
47. Uda Y, Hirano T, Son G, Imuro Y, Uyama N, Yamanaka J, Mori A, Arii S, Fujimoto J. Angiogenesis is crucial for liver regeneration after partial hepatectomy. *Surgery*. 2013;153:70–7.
48. LeCouter J, Moritz DR, Li B, Phillips GL, Liang XH, Gerber HP, Hillan KJ, Ferrara N. Angiogenesis-independent endothelial protection of liver: role of VEGFR-1. *Science*. 2003;299:890–3.
49. Hess A, Gentile SD, Ben Saad A, Rahman RU, Habboub T, Pratt DS, Mullen AC. Single-cell transcriptomics stratifies organoid models of metabolic dysfunction-associated steatotic liver disease. *EMBO J*. 2023;42:e113898.
50. Osonoi S, Takebe T. Organoid-guided precision hepatology for metabolic liver disease. *J Hepatol*. 2024;80:805–21.

Publisher's Note

Springer Nature remains neutral with regard to jurisdictional claims in published maps and institutional affiliations.